


Article

# Application of a statistical and linear response theory to multi-ion Na<sup>+</sup> conduction in NaChBac

William A.T. Gibby<sup>1\*</sup> , Olena Fedorenko<sup>2,4</sup>, Carlo Guardiani<sup>1,3</sup>, Miroslav Barabash<sup>1</sup>, Thomas Mumby<sup>1</sup>, Stephen Roberts<sup>4</sup>, Dmitry Luchinsky<sup>1,5</sup> and Peter V.E. McClintock<sup>1\*</sup>

<sup>1</sup>Department of Physics, Lancaster University, Lancaster LA1 4YB, UK.

<sup>2</sup>School of Life Sciences, University of Nottingham, Nottingham NG7 2UH, UK.

<sup>3</sup>Department of Mechanical and Aerospace Engineering, Sapienza University, Rome, Italy.

<sup>4</sup>Division of Biomedical and Life Sciences, Lancaster University, Lancaster LA1 4YQ, UK.

<sup>5</sup>SGT Inc., Greenbelt, MD, 20770, USA.

\* Correspondence: w.gibby@lancaster.ac.uk; p.v.e.mcclintock@lancaster.ac.uk

Version February 3, 2021 submitted to Entropy

**Abstract:** Biological ion channels are fundamental to maintaining life. In this manuscript we apply our recently developed statistical and linear response theory to investigate Na<sup>+</sup> conduction through the prokaryotic Na<sup>+</sup> channel NaChBac. This work is extended theoretically by the derivation of ionic conductivity and current in an electrochemical gradient, thus enabling us to compare to a range of whole-cell data sets performed on this channel. Furthermore, we also compare the magnitudes of the currents and populations at each binding site to previously published single-channel recordings and molecular dynamics simulations respectively. In doing so, we find excellent agreement between theory and data, with predicted energy barriers at each of the four binding sites of  $\sim 4, 2.9, 3.6, \text{ and } 4kT$ .

**Keywords:** Ion channel; Statistical theory; Linear response; Ionic transport; NaChBac

## 1. Introduction

Biological channels are natural nanopores that passively transport ions across cellular membranes. These channels are of enormous physiological and pharmacological importance, and so investigation of their transport properties is an area of great interest and research. For example, Na<sup>+</sup> channels play a key role in the generation of the action potential [1–3]. Furthermore, artificial nanopores are primarily designed for their transport functionality which can be informed by our understanding of biological channels.

A primary function of these channels is their ability to discriminate effectively between ions, whilst still conducting them at high rates. An example is NaChBac from *Bacillus halodurans*, which is the first bacterial voltage-gated sodium channel (Nav) to have been characterised, and thus is a prokaryotic prototype for investigating the structure–function relationship of Nav channels [4]. It conducts ions at rates of  $10^7 \text{ s}^{-1}$  despite having permeability ratios favouring Na<sup>+</sup> over K<sup>+</sup> and over Ca<sup>++</sup>. Recently we reported these values to be *at least* 10:1 and 5:1 respectively [5]. **In fact from the reversal potential the Na<sup>+</sup>/K<sup>+</sup> permeability ratio is found to be 25:1, which is closer in agreement but still less than [6] who found the ratio to be 170:1. This contrasts with potassium channels such as KcsA where selectivity is reversed, favouring K<sup>+</sup> over Na<sup>+</sup> at 1000:1 [7].** The channel itself is formed from several coupled subsystems, but we focus on the selectivity filter (SF) which is the primary region responsible for selectivity between ions. The SF can readily be mutated to generate a range of conducting (and non-conducting) channel types which exhibit different selectivity and conductivity properties compared to those exhibited by the wild-type (WT) channel (see [5]).

30 The SF has the amino acid<sup>1</sup> sequence TLESWAS, and thus shares the TxExW sequence with  
31 eukaryotic calcium channels [6]. Unfortunately, a crystal structure of NaChBac is not available.  
32 However, Guardiani. et. al. [8–10] applied homology structural modelling to produce a structure of  
33 NaChBac that we will use in this publication. We conduct a variety of different Molecular Dynamics  
34 (MD) simulations (see Fig. 1) to explore its properties. During simulation the SF was found to have  
35 an average radius  $R_c \sim 2.8\text{\AA}$ , length  $L_c \sim 12\text{\AA}$  and 4 binding sites for conducting  $\text{Na}^+$  ions labelled  
36 S1-4 from the intra- to the extra-cellular side respectively. The conduction mechanism was found  
37 to involve knock-on between at least 2, if not 3, ions. Each binding site has a volume, as estimated  
38 in Table 1, whose sum gives the total volume of the pore  $V_c$ . The first two sites are formed at the  
39 backbone carbonyls of the threonine and leucine residues respectively. S1 is wider than the average  
40 pore radius with diameter  $3.06\text{\AA}$ , but S2 has the average pore radius of  $2.8\text{\AA}$ . As a result, these two  
41 sites accommodate the primary hydration shell with around 5-6 waters per ion, and thus prevent  
42 bare ion-protein interaction. S3 is of approximately the same size as S2, but the ion only interacts  
43 with four waters because it also interacts directly with the glutamate ring. The fourth site is formed  
44 on the extracellular side from the side chain of the serine residues and a sodium ion here has a 40%  
45 probability of interacting with one or two serines and a 60% probability of being fully hydrated by  
46 water. This is in stark contrast to the narrower potassium channels where  $\text{K}^+$  ions are almost fully  
47 dehydrated as they permeate the pore. The  $\text{Na}^+$  occupancies at each site have been determined by  
48 molecular simulation using 0.5M bulk solutions. Both S1 and S4 have energy minima that are higher  
49 in energy than S2,3 and so are less likely to be occupied. In fact the average occupancy of S1,4 is only  
50 around half that of the most occupied site S2 (see Fig. 7 (c)).

51 These results are consistent with the results of MD simulations that have been performed on  
52 a variety of similar bacterial NaV channels. Chakrabarti et al [11] conducted a  $21.6\ \mu\text{s}$ -long MD  
53 simulation of NavAb, observing a variable number of ions in the pore, mainly 2 or 3 (rarely 4) and  
54 spontaneous and reversible ionic diffusion along the pore axis. Ulmschneider et al. [12] simulated the  
55 open state of the pore domain of NavMs with a voltage applied, and calculated the conductance which  
56 at  $\sim 33\text{pS}$  was in agreement with experimental results.

57 The SF has a nominal charge of  $-4e$  arising from the fixed glutamate ring. However, determining  
58 the exact charge contribution from these pores is challenging due to the potential partial charges from  
59 remaining uncharged amino acids and the protonation that may occur at physiological pH levels. That  
60 latter is suspected to be true in voltage-gated  $\text{Ca}^{++}$  channels which share a ring of glutamates [13,14].  
61 As a result, protonation of the glutamate ring in Navs has been studied fairly extensively [5,15–18].  
62 Corry and Thomas [16] investigated the pore when only a single glutamate residue was protonated.  
63 The slightly protonated pore showed little difference in the potential of mean force vs. the normal  
64 pore. However, the doubly-protonated state showed a larger barrier for permeation to the pore, and  
65 reduced affinity for ion binding. Boiteux et. al.[17] found a slight difference in the average number of  
66  $\text{Na}^+$  ions in the SF at 2.3 and 2.0 in the fully deprotonated and slightly-protonated states, respectively;  
67 however, both states were conducting. In simulations with two protonated residues, the authors  
68 observed the existence of a non-conducting state forming as a result of stable hydrogen bonds between  
69 the glutamates. As the number of protonated residues increased to 3 and 4, Chloride  $\text{Cl}^-$  ions started  
70 to bind and the pore became non-conductive for  $\text{Na}^+$ . A similar study with shorter biased simulations  
71 suggested that protonation of a single Glu residue would diminish the conductance [15]. Meanwhile, a  
72 recent [18] study found that, at physiological pH, the pore may exist in the full deprotonation state but  
73 that it could also exist in the single or double-protonation states as well. Furthermore, the calculated  
74 pKa value decreases with each additional bound ion, implying that the presence of ions inside the pore  
75 leads to protonation of the SF. Thus, in [5] we introduced the notion of an effective charge describing

---

<sup>1</sup> Here: T=threonine, L=Lecucine, E=glutamte, S=serine, W=tryptophan, A=alanine and x highlights where the sequence is not conserved and can be several possible amino acids.

76 the total charge in the pore as felt by the conducting ion, and its values were estimated by fitting  
77 Brownian dynamics simulations to experimental data for wild-type (WT) NaChBac and for a large  
78 selection of mutants. In our earlier work we studied NaChBac and its mutants theoretically and by  
79 Brownian dynamics simulation [5,19].

80 In earlier publications [5,20], we reported studies of  $\text{Na}^+$  and  $\text{Ca}^{++}$  permeation in NaChBac,  
81 using Brownian dynamics models. The key result of modelling was that ionic conduction is analogous  
82 to electron transport in a quantum dot. As a function of the value of fixed charge, we observed a set  
83 of resonant conduction peaks separated by regions of blockade where the ions could not enter/leave  
84 the pore. This phenomenon is called *ionic Coulomb blockade* (ICB) [21], by analogy with (electronic)  
85 Coulomb blockade in quantum dots, for which the physics and the governing equations are essentially  
86 the same. Each resonant peak corresponds to an  $n \rightarrow n + 1$  barrier-less transition, which is of the  
87 knock-on kind when  $n > 0$  [22], and the regions of blockade are when the charge carrier cannot pass.  
88 The occurrence of ICB has also been confirmed experimentally in artificial nanopores [23,24]. Although  
89 the ICB model explained immediately the role of the fixed charge, and accounted convincingly for  
90 the effect of mutations in which the fixed charge is altered, it is only a good approximation when  
91 electrostatic forces are dominant i.e. for divalent and trivalent ions. Furthermore, it doesn't contain  
92 affinities in the pore or excess chemical potentials in the bulk and so it cannot describe selectivity  
93 between ions of the same charge. It is also not connected to the results of Molecular simulation (MD)  
94 or the structure, and it cannot describe the absolute magnitude of the permeating current.

95 To provide a more accurate description, we needed a more fundamental model. We therefore  
96 developed a kinetic model [19], to investigate  $\text{Na}^+$  vs.  $\text{K}^+$  selectivity. This model was based on a  
97 simplified two site model of NaChBac and it was made self-consistent through the form of its transition  
98 rates. These were chosen such that the kinetic model and an earlier statistical and linear response  
99 theory had the same form of conductivity at low voltages. However, this did not include the complete  
100 structure or any comparison to results from MD simulation. It also did not include the binding site  
101 conductivities, or account for the correlations between ions at different binding sites. These two  
102 properties are expected to be important for fully describing the permeation properties and making  
103 quantitative predictions of the function of biological channels because it is known that small mutations  
104 in structure can lead to significant changes in function e.g. [5,25,26]. This was shown in [27], where we  
105 introduced a statistical and linear response theory fully accounting for structure and the properties of  
106 each binding site, and used it to analyse a point mutation in KcsA exploring the reasoning behind its  
107 drop in conductivity and occupancy.

108 In the present paper, we apply this recently developed statistical and linear response theory  
109 [27] to NaChBac with a more accurate model based on the structure introduced in [8]. The theory  
110 will include all four binding sites and their estimated volumes and surface areas, and the excess  
111 chemical potentials at each site. Furthermore, we extend this theory by deriving the conductivity at  
112 linear response in the presence of an *electrochemical* gradient. The theory is successfully compared  
113 to experimental single-channel and whole-cell recordings (some of which published in [5,19]), and  
114 results from MD simulations [8]. Finally, the theory allows us to make quantitative predictions of the  
115 current-concentration and current-voltage relations, and the effective open probability of the channel;  
116 as a function of the energy profile, experimental bulk concentration and structure of the pore.

117 In what follows, with SI units  $e$  is the unit charge,  $T$  the temperature,  $z$  the ionic valence, and  $k$   
118 Boltzmann's constant.

## 119 2. Experimental Methods and Data

120 To apply the theory to NaChBac, and to compare with experimental recordings and make  
121 predictions, we consider two experiments. For further details of the experimental methods, including  
122 generation of the mutant channels and their expression, as well as details of the electro-physiological  
123 experiments, we refer to [5], and here we only present a concise summary. The first of these data  
124 sets is single-channel current-voltage recordings originally published in [19]. In these experiments

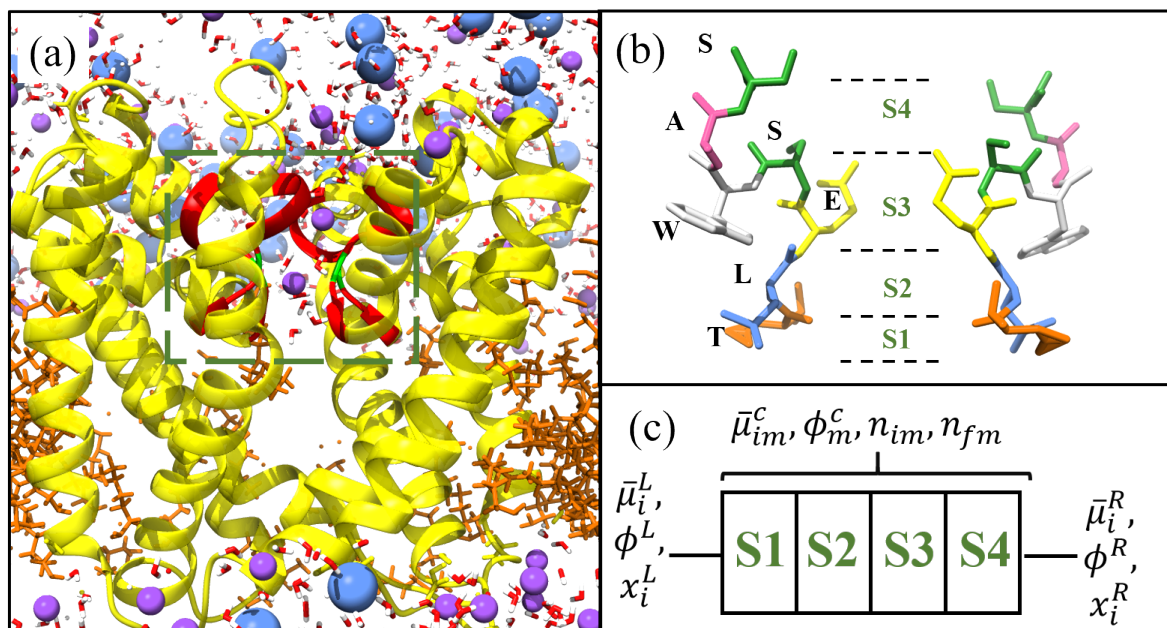


**Figure 1.** Structure of NaChBac [8] visualised using chimera [28]. (a) Yellow ribbons denote the protein spanning a lipid membrane (orange strands) between two aqueous ionic solutions. The SF is located within the box and highlighted by the red ribbons. The charged glutamates in the SF are highlighted green, and  $\text{Na}^+$  (purple), and  $\text{Cl}^-$  (blue) ions alongside water molecules are included. (b) Structure of the SF for NaChBac with each amino acid highlighted and labelled by colour. The positions of the binding sites are included and labelled S1-S4 from the intra- to the extra-cellular side respectively. In (c) we show the lattice model used to define the system.

125 identical bath and pipette solutions containing (in mM: 137 NaCl, 10 HEPES and 10 glucose, pH 7.4  
 126 adjusted with 3.6 mM NaOH) were used. Single-channel recordings are possible because  $\text{Na}^+$  is the  
 127 preferred substrate with sufficiently high conductance to provide a single-channel current amplitude  
 128 which significantly exceeded noise (i.e. a favorable signal-to-noise ratio). In Fig. 2 (a) we plot the  
 129 current-voltage curve, and in (b,c) we provide a current-time trace made at +100 mV. Trace (c) begins  
 130 at the end of trace (b). There are at least three active channels passing currents with the magnitudes  
 131 shown by the dashed lines.

132 In the second series of experiments we performed whole-cell current measurements through  
 133 NaChBac, in different  $\text{Na}^+/\text{K}^+$  concentrations (see Fig. 3). The black and purple curves in (a) (and  
 134 the curve in (c)) i.e. with 0M and 0.14M of NaCl solutions in the bath solution respectively (or 0.14M  
 135 and 0M of KCl), were published in [5]. An identical experiment on a mutant was performed and  
 136 described in [19]. In each case, the pipette solution contained (in mM) 120 Cs-methanesulfonate,

Site	Estimated Average Radius	Estimated Length	Estimated Surface Area	Estimated Volume
S1	3.06Å	3Å	116(Å) <sup>2</sup>	117(Å) <sup>3</sup>
S2	2.77Å	4Å	126(Å) <sup>2</sup>	129(Å) <sup>3</sup>
S3	2.75Å	3Å	90(Å) <sup>2</sup>	80(Å) <sup>3</sup>
S4	2.77Å	2Å	78(Å) <sup>2</sup>	63(Å) <sup>3</sup>
Mean	2.8Å	3Å	103(Å) <sup>2</sup>	97(Å) <sup>3</sup>

**Table 1.** Table of averaged radii and length of each binding site, obtained through the homology based structural model of NaChBac from [8]. The corresponding surface areas and volumes were estimated by assuming that each site was spheroidal in shape. The binding site is identified from a minima in the potential of mean force (PMF), and its length is estimated from the distance between maxima in the PMF. The radius is estimated from the average calculated radius in this region. These lengths and radii are given in the table.

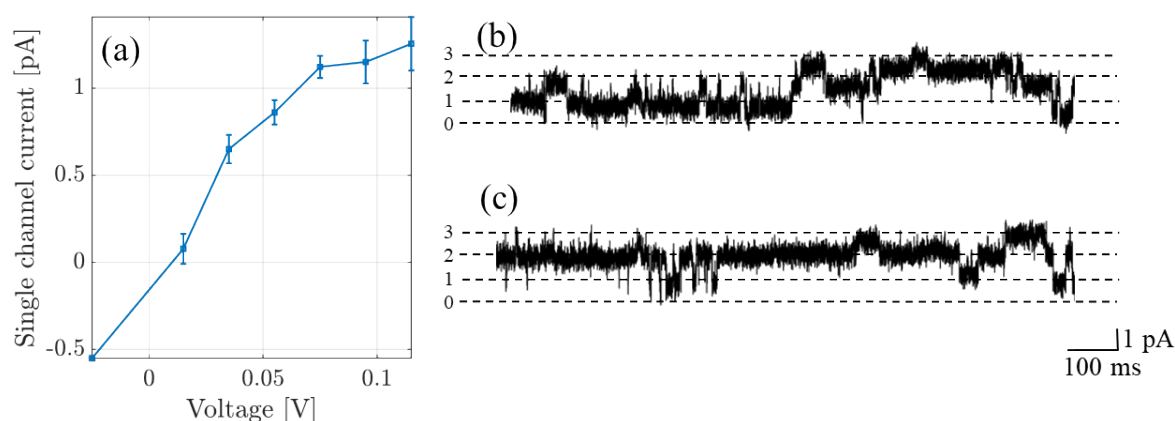


**Figure 2.** (a) Single channel currents recorded from NaChBac (originally published in [19]). (b) and (c) The original recording made at +100 mV in the 140 mM NaCl solution; the trace contains contributions from at least three active channels; and (c) represents a continuation in time of trace (b). The dashed lines show the amplitude level per channel, the numbers on the ordinate denoting the number of open channels.

137 20 Na-gluconate, 5 CsCl, 10 EGTA, and 20 HEPES, pH7.4 adjusted with 1.8 CsOH, meanwhile the  
 138 bath solution contained (in mM); 137NaCl, 10 HEPES and 10 glucose, pH 7.4 (adjusted with 3.6 mM  
 139 NaOH). Permeability to  $K^+$  was investigated by incrementally replacing the NaCl bath solution with  
 140 an equivalent KCl solution such that the total ionic concentration was fixed at 140 mM. Total current  
 141 across the cell was then normalized and, because one can assume that the total number of channels,  
 142 their type and their open probability is conserved in each cell for the duration of the recording, it can  
 143 effectively be modeled as a single channel. This normalization was with respect to the absolute value  
 144 of peak current and is shown in (a) of Fig. 3. In (b) we show the current-concentration behaviour  
 145 at -10mV, which corresponds to the peak current. The reversal potential is plotted in (c); in cases  
 146 where inward current was not detected, estimated values were determined from the voltage at which  
 147 outward current could be detected. Finally, in (d) and (e) we provide the corresponding current-time  
 148 traces.

149 Since NaChBac is highly impermeable to  $K^+$  and  $Cl^-$  we have neglected the presence of these  
 150 ions in the pore and in our theory we shall simply consider a single ion species i.e.  $Na^+$  inside the pore.

### 151 2.1. Comparison of NaChBac structures

152 In this subsection we shall compare the structure of NaChBac from the homology model which  
 153 was used in [8], and the Cryo-EM structures 6vx3.pdb and 6vwx.pdb from [4].

154 In Fig. 4 we provide an overlay of the homology model (yellow ribbons) and the 6vx3.pdb  
 155 structure (green ribbons), using all of the backbone atoms. (a) provides the overlay of the whole  
 156 pore and (b) provides a snap-shot of the selectivity filter (SF). From visual inspection there is clearly  
 157 good agreement between the structures. In the pore the root-mean-square distance between structures  
 158 (computed using the backbone atoms) is  $17.47\text{\AA}$  and  $7.14\text{\AA}$  in the SF.

159 To further explore these structures we considered the pore radius which can be compared using  
 160 the HOLE program. In Fig. 5 we show a comparison between structures. The homology model is  
 161 more open than the Cryo-EM structures (6vx3 and 6vwx) both at the level of the cytosolic mouth  
 162 (minimum centered on  $z = -15\text{\AA}$ ) and in the region of the SF (around  $z = 0 - 12\text{\AA}$ ). This is confirmed  
 163 by volume filling representations of the pores which show a bottleneck close to the cytosolic mouth of  
 164 6vx3. The SF of 6vwx is narrower because the SF is occupied by two  $Na^+$  ions, and these attract the  
 165 side chains of the glutamates and the backbone carbonyls of the leucines, moving them towards the  
 166 centre of the pore. Hence, there are two distinct minima in the pore radius which cannot be spotted  
 167 in the radius profile of the homology model because this structure was obviously empty. However,

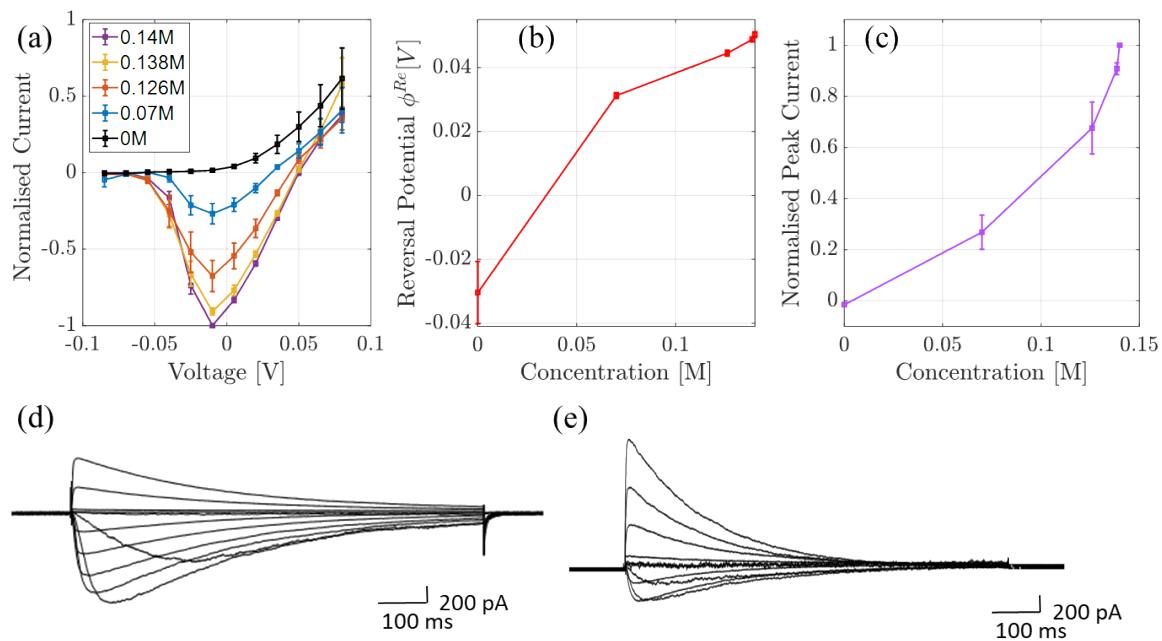


**Figure 3.** (a) Mean peak whole cell voltage-current relationships from cells expressing NaChBac channels, obtained in the bath solution with decreasing Na<sup>+</sup> content ranging from 140 mM to 0 mM (with NaCl being replaced with equimolar KCl). The peak currents were determined from time *vs.* current traces (examples shown in parts (d) and (e)). Peak currents are normalized to the peak current recorded from the same cell in 140 mM NaCl-containing solution in the absence of K<sup>+</sup>; error bars represent the SEM of mean values determined from at least 4 independent cells. In (b) we show mean reversal potentials ( $\pm$  SEM) determined from data plotted in part (a). In cases where inward current was not detected, the reversal potential was assumed to be the voltage at which outward current could be detected. In (c) we plot the mean ( $\pm$  SEM) peak whole cell current (determined from data plotted in part a) as a function of Na concentration. Parts (d) and (e) are examples of time-dependent NaChBac currents recorded in 140 mM NaCl (d) and 130 mM NaCl and 10 mM KCl (e).

168 the fact that the SF in 6v3 (whose SF is empty) is also narrower than that of the model suggests that  
 169 the structural differences might reflect different functional states in the channel cycle. In fact in the  
 170 paper [4], Gao comments on the narrow radius of the cytosolic mouth, and on the arrangement of the  
 171 Voltage Sensor Domain, suggesting that these structures might represent an inactivated conformation  
 172 of the pore. By contrast, our homology model was built using the fully open conformation of NavMs  
 173 from *Magnetococcus sp.* (PDB ID: 4F4L) as a template. As a result, our homology model probably  
 174 represents an open conformation of NaChBac. This choice was deliberately taken on the assumption  
 175 that an open conformation would be more suitable for the computational study of permeation and  
 176 selectivity. In summary, the good agreement in overlaid structures, along with the choice to use an  
 177 open conformation of NavMs as a template, makes us confident our model is a reliable system for the  
 178 study of the selectivity and permeation of NaChBac.

### 179 3. Theory

To model the SF we consider a system comprised of a pore thermally and diffusively coupled at either entrance to bulk reservoirs. This system and the effective grand canonical ensemble was considered and rigorously derived for multi-ion species in [27], and here we only present the necessary details needed to describe a single-species system. This pore is represented as a 1-dimensional lattice with 4 sites that may be occupied by a single ion at most. These are labelled S1-4 starting from the intracellular side in (c) of Fig. 1. This figure also provides in (a) an overview of the system and (b) a snapshot of the SF which is highlighted by the red ribbons in (a). Clearly each configuration of Na<sup>+</sup>

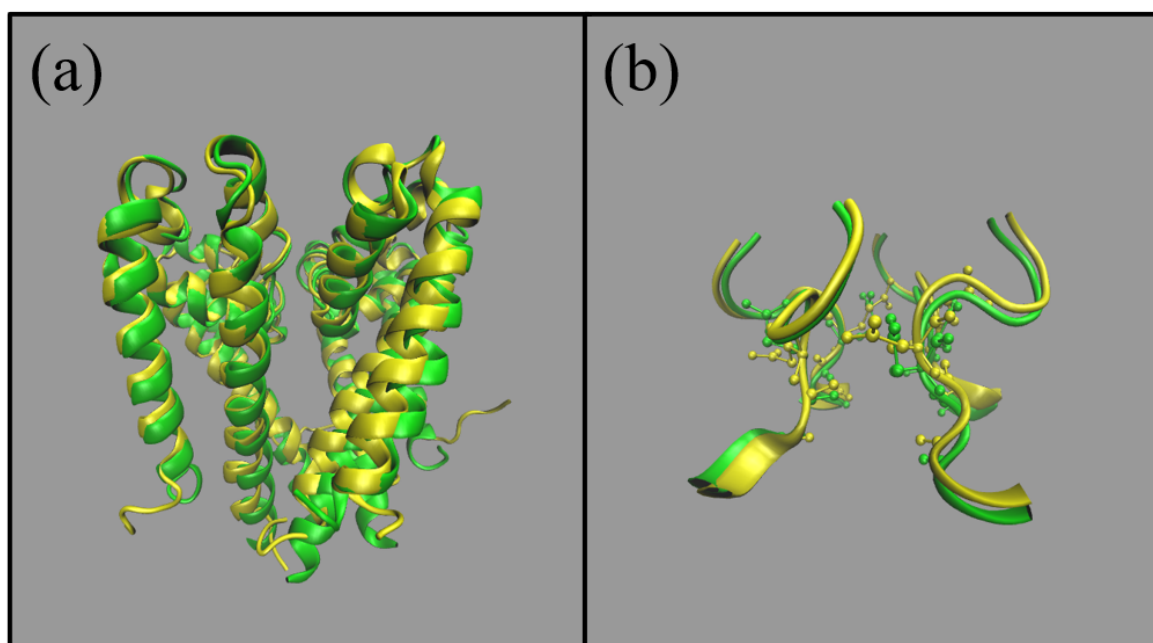


**Figure 4.** Comparison of NaChBac structures from the homology model (yellow) introduced in [8] and the Cryo-Em structure in green (6vx3.pdb) from [4]. (a) represents the whole pore and (b) is a snapshot of the (half) selectivity filter.

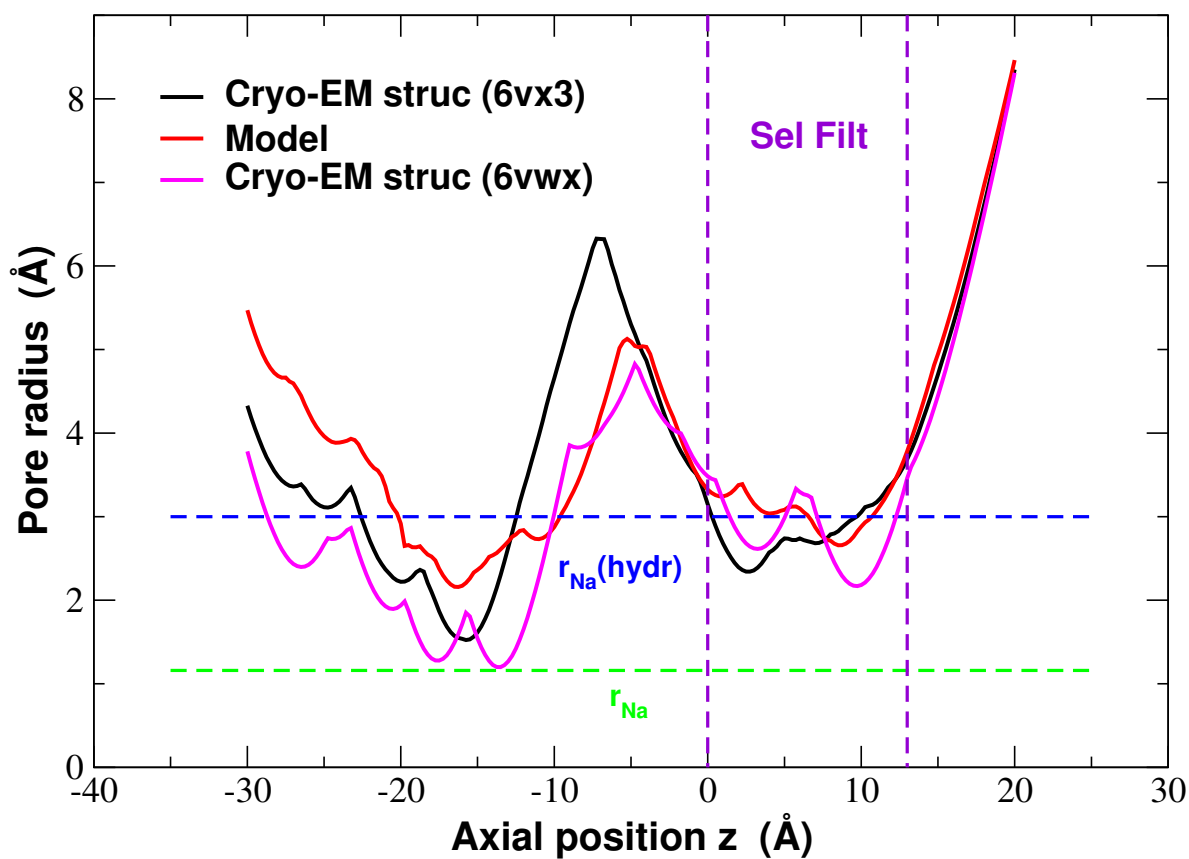


**Figure 5.** Comparison of average pore radius in the homology model structure (red) [8] and Cryo-EM structures 6vx3.pdb (black) and 6vwx.pdb (pink) [4]. The green and blue dashed lines denote the ionic  $\text{Na}^+$  and hydrated  $\text{Na}^+$  radii, respectively, and the purple dashed lines at  $z = 0, 13\text{\AA}$  highlight the selectivity filter region.

ions in the pore represent a distinct state of the system with total state space  $\{n_j\}$ . In this system ions inside the pore interact electrostatically with each other and charges on the surface of the pore via  $\mathcal{E}$ . Furthermore, they also interact locally at each binding site,  $m$ , via short-range contributions  $\bar{\mu}_m^c$  and may experience an applied potential  $\phi_m^c$ . Thus, with only  $\text{Na}^+$  in the pore we can write the following distribution function,  $P(\{n_j\})$ ,

$$P(\{n_j\}) = \mathcal{Z}^{-1} \frac{(x_{\text{Na}}^b)^{n_{\text{Na}}}}{n_0! n_{\text{Na}}!} \exp[-(\mathcal{E}(\{n_j\}) - \sum_m n_{\text{Na}m} (\Delta\bar{\mu}_{\text{Na}m} + ez\Delta\phi_m^b))/kT]. \quad (1)$$

180 We have introduced  $\Delta$  to denote the difference between bulk and site  $m$  in the pore such that  
 181  $\Delta\bar{\mu}_m^b = \bar{\mu}^b - \bar{\mu}_m^c$  and  $\Delta\phi_m^b = \phi^b - \phi_m^c$ . In these cases  $\bar{\mu}$  and  $\phi$  denote the excess chemical potential and  
 182 applied voltage in the bulk or at site  $m$  respectively. The prefactor contains factorial terms due to  
 183 the indistinguishability of ions  $n_{\text{Na}}$  and empty sites  $n_0$  in the pore, and  $x_{\text{Na}}$  denotes the mole fraction.  
 184 For clarity we will drop the Na subscript. The necessary statistical properties such as site or pore  
 185 occupancy can be derived from the partition function  $\mathcal{Z}$  or Grand potential  $\Omega = -kT \log(\mathcal{Z})$ .

In [27] we demonstrated that the response to an applied electric field can be calculated following Kubo and Zwanzig [29–31]. We showed that the susceptibility density at each site can easily be derived and related to the conductivity at each site following the Generalised Einstein relation. The total conductivity through the pore is thus calculated by summing the reciprocals of the site-conductivity, in analogy to resistors in series. As a result all sites must be conducting for the total conductivity to be non-negligible. This effect partly explains the reduced conduction of a KcsA mutant [25], although we have to be mindful that the overall pore charge also decreases, increasing the overall energy barrier for conduction, and contributing to the reduced conductivity. We shall extend this derivation here by considering the response to an electrochemical gradient comprised of an electric potential gradient  $\delta\phi$  and a concentration gradient  $\delta c$ . We shall assume that both bulk reservoirs are perturbed symmetrically so that the left (+) and right (-) electrochemical potentials,  $\mu^b$ , can be written,

$$\mu^b = kT \log((c \pm \delta c/2)/c_w) + \bar{\mu}^0 + qz\phi^0 \pm ez\delta\phi/2. \quad (2)$$

Where:  $c_w$  is the concentration of the solvent which is much larger than that of the ions at around  $\sim 55M$ , and  $c$  is the concentration of the solute,  $\bar{\mu}^0$  is the equilibrium bulk excess potential which we assume to be unperturbed by the electrochemical gradient and  $\phi^0$  is the equilibrium electrical potential (which we will consider to be 0). In the following derivation we will write  $c/c_w$  as the mole fraction  $x$ . Thus following [27] we can write the following free energy,  $G(\{n_j\}, \delta\phi, \delta x)$ , in the presence of this gradient by linearising  $\mu^b$  about small  $\delta c$ ,

$$G(\{n_j\}, \delta\phi, \delta x) = \mathcal{E}(\{n_j\}) - \sum_{m=1}^M n_m (kT \log(x) + \Delta\bar{\mu}_m^0 \pm \frac{kT}{2c} \delta c \pm ezv_m^b \delta\phi) + kT \ln(n_0)! + kT \ln n!. \quad (3)$$

In this expression we have rewritten  $\delta\phi_m^b = v_m^b \delta\phi$  where  $v_m^b$  is a function representing the fraction of the voltage drop to move from either the left or right bulk to site  $m$  in the pore (see [27] for details). In a symmetrically distributed pore (which we assume), the average of  $v_m^b$  is equal to 1/2. In this regime the probability distribution function can be written as

$$P(\{n_j\}, \delta\phi, \delta c) = Z^{-1} \frac{1}{n_0! n!} \exp[-(\mathcal{E} - \sum_m n_m (\Delta\bar{\mu}_m^0 \pm ezv_m^b \delta\phi \pm \frac{kT}{2c} \delta c))/kT]. \quad (4)$$



Here the partition function  $Z$  is defined in the standard manner from the conservation of probability and distinguished from the equilibrium partition function  $\mathcal{Z}$ . Both the free energy and distribution function can also be expressed in terms of the chemical gradient  $\eta^L - \eta^R$  because

$$kT \log(x^L/x^R) = \delta\eta = \frac{kT}{c} \delta c. \quad (5)$$

The distribution (4) can be linearised about both small  $\delta\phi$  and  $\delta c$ . When calculating the average particle density at each site  $\langle n_m \rangle_{\delta c, \delta\phi} / V_m$ , where  $V_m$  is the site volume, one can obtain relations for the susceptibilities due to the electrical gradient  $\chi_m^{\delta\phi}$  and the chemical or concentration gradient  $\chi_m^{\delta\eta}$ . The former is defined in [27], **since we assume a symmetrical pore** the latter is defined as,

$$\chi_m^{\delta\eta} = \frac{1}{2kT} \left( \left\langle n_m \left( \sum_m n_m \right) \right\rangle - \left\langle \left( \sum_m n_m \right) \right\rangle \langle n_m \rangle \right) \frac{1}{V_m} \quad (6)$$

It is worth noting that this expression is similar to  $\chi_m^{\delta\phi}$  and is proportional to the variance of particle number at site  $m$  plus the covariance between sites  $m$  and the remaining sites in the pore. These susceptibilities are also proportional to the electrical conductivity,  $\sigma_m$ , at each binding site, which can be defined from the Einstein relation as:  $\sigma_m = q^2 D_m \chi_m$  where  $D_m$  and  $\chi_m$  correspond to the diffusivity and susceptibility at each site respectively. As a result, the total current across the pore can be calculated as [27]

$$I = \left( \sum_m \frac{1}{\frac{A_m}{L_m} \sigma_m} \right)^{-1} (\delta\phi + \delta\eta/q), \quad (7)$$

where we recall that  $\delta\phi$  is the voltage gradient in  $V$ ,  $\delta\eta$  is the chemical gradient in  $kT$ , and  $A_m$  and  $L_m$  are the surface area and length of site  $m$  respectively. Finally, the conductivity at each site is calculated from

$$\sigma_m = ze^2 D_m (\chi_m^{\delta\phi} + \chi_m^{\delta\eta}), \quad (8)$$

186 which is a function of the equilibrium bulk chemical potential.

#### 187 4. Application to NaChBac

188 In Fig. 6 (a) we consider the free energy spectra for selected (most favoured) pore configurations  
 189 of NaChBac calculated from Eqn. (3) (when  $\delta\phi = 0$  and  $\delta c = 0$ ). We consider 0.14M NaCl solutions,  
 190 and 0-3 ions inside the pore. In Eqn. (3) the total electrostatic energy,  $\mathcal{E}$ , is calculated by approximating  
 191 the pore as a capacitor of total charge  $n_f$  and capacitance  $C$  taking the form  $\mathcal{E} = U_c(n_f + n)^2$  where  
 192  $U_c = \frac{e^2}{2C}$  [20,32],. **Since the permittivity of water inside the pore is not known (though it must be less**  
 193 **than the bulk value of 80) we consider  $U_c = 10kT$ .** This approximation is discussed in detail in [27].  
 194 The energy spectra are parabolic vs.  $n_f$ , and each  $n$ -ion state has multiple configurations (15 in total)  
 195 and we only highlight the most favoured. These states are determined by **the values of  $\Delta\bar{\mu}_{Nam}$ , and**  
 196 **their exact values are determined from fitting to experimental data (see subsection 4.1).** Differences in  
 197 this term lead to energy splitting between possible configurations **because the site occupied, in addition**  
 198 **to the total number of ions inside the pore, determines the energy**, conducting states correspond to the  
 199 degeneracies where the lowest energy levels intersect, cf. [22], and this was shown to be the case in  
 200 KcsA [27]. In NaChBac, the circle highlighting the 2-3 resonant transition occurs at around  $n_f \sim -2.7$ .  
 201 Importantly, this differs from  $n_f = -2.5$ , suggesting that the the 3rd-ion faces an energy barrier to  
 202 enter each site. If the concentration of the solutions was increased the energy barrier would decrease  
 203 and the location of the resonant conduction would shift along the abscissa towards  $n_f - 2.5$ . It is worth  
 204 reiterating that  $n_f$  here represents the total pore charge, and so differences from the fixed glutamate  
 205 ring charge of  $-4e$  can be explained from the additional contribution of all other charges and possible  
 206 protonation inside the pore. Extended discussions of this point are provided in [5,15–18].

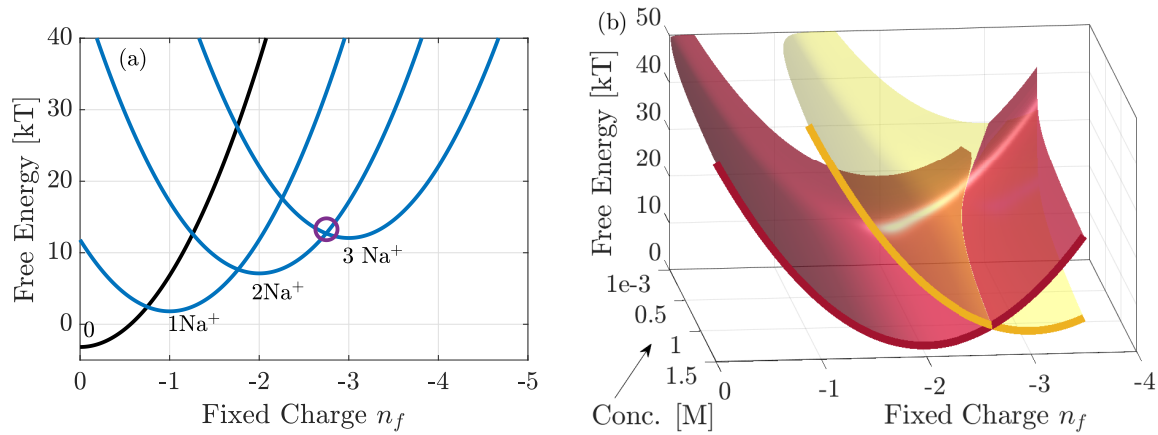


**Figure 6.** Free energy of the favoured states, plotted with  $\Delta\bar{\mu}_{Na,1-4} \sim 2.3, 3.4, 2.8, 2.4kT$ . In (a) it is plotted *vs.*  $n_f$  with 0.14M NaCl bulk solutions and in (b) *vs.* both  $n_f$  and bulk concentration. In (a) the blue curves correspond to the occupied  $n > 0$  states of the pore, and black denotes the empty state. The purple circle highlights the location at which the two most favoured 2 and 3 ion states coincide, and we see that at  $n_f = -2.5$  there is a small energy barrier. As bulk concentration increases this energy barrier reduces and the purple circle would shift towards  $n_f = -2.5$ . This is further clarified by (b) which shows only the 2 and 3 ions states.

207 In Fig. 6(b) we plot the energy spectra of the favoured 2 and 3-ion states, *vs.*  $n_f$  but also *vs.* bulk  
 208 concentration. From the explanation above it is clear that the latter affects the value of  $n_f$  at which  
 209 the two energy levels intersect. At low concentrations the energy barrier to add an ion to the pore is  
 210 large. Thus, strong negative pore charge is required to reduce the barrier to attract the ion. Conversely  
 211 at large concentrations the barrier is small and so less negative charge is needed. Thus one would  
 212 expect the experimental current to be larger for measurements at higher concentrations, if these could  
 213 be made.

214 To obtain the values of  $\Delta\bar{\mu}_{Na,1-4}$  we performed fitting to two data sets, and this will be explained  
 215 in the following subsection.

#### 216 4.1. Comparison to Single channel data and MD

217 The values of  $\Delta\bar{\mu}_{Na,m}$  used in Fig. 6 are obtained by fitting, performed using the LSQCURVEFIT  
 218 function in Matlab. We fit theory to the equilibrium site occupancies  $\langle n_{Na,m} \rangle$  calculated from simulation  
 219 data [8] (see Fig. 2 (c)), and the current at 35 mV. Current is needed here so that we can ensure it is of  
 220 the correct order of magnitude. We also note that the difference in bulk NaCl concentration between  
 221 the current and occupancy data is taken into account during fitting. To minimise the number of free  
 222 parameters we also assumed that the diffusivity in the pore was constant, and equal to a tenth of  
 223 the bulk value at  $\sim 1.33 \times 10^{-10} \text{m}^2 \text{s}^{-1}$ , and calculated  $\Delta\bar{\mu}_{Na,m}$ , relative to  $n_f = -2.5$ . The diffusivity  
 224 is expected to be smaller within a confined pore due to the nature of the binding sites [33,34] and,  
 225 although this value may appear small, it produces a barrier-less conduction rate through the pore of  
 226  $\sim 0.9 \times 10^8$  ions per second which is of the order of tens of pA. We choose  $n_f = -2.5$  because the  
 227 electrostatic contribution to add a third ion is zero i.e.  $\mathcal{E}(3) - \mathcal{E}(2) = 0$ .

228 Both data sets are in excellent agreement with the theory, with currents only starting to differ at  
 229 relatively large voltages when the experimental data deviate from Ohmic behaviour. Clearly beyond  
 230 this regime, the system is far from equilibrium and our theory will need to be extended accordingly.  
 231 After fitting we obtain  $\Delta\bar{\mu}_{Na,1-4} \sim 2.3, 3.4, 2.8, 2.4kT$  when  $n_f = -2.5$ , with the sum of squared  
 232 residuals being small at  $10^{-4}$ . When the concentration is 0.14M the ions face the following barriers  
 233 to enter each site:  $\sim 4.0, 2.9, 3.6, 4.0kT$ . These barriers are fairly similar to each other, although it is  
 234 clear that S2 is the more favoured site and this is shown by its occupancy. As already discussed and  
 235 observed in Fig. 6, the energy barrier at each site reduces when the bulk concentration increases from

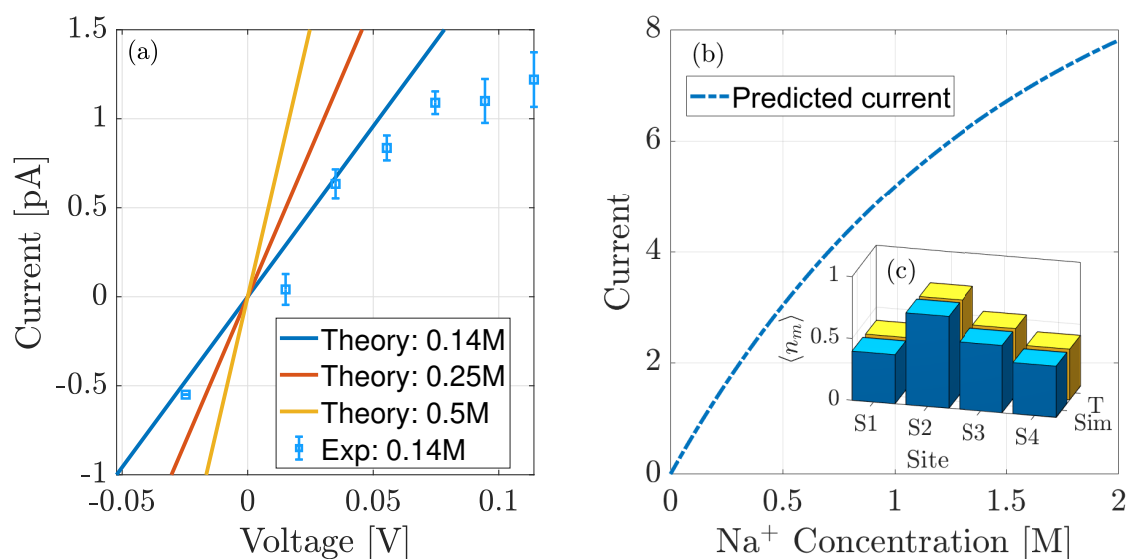


**Figure 7.** (a) Comparison of theoretical current *vs.* experimental data (squares) taken from [19] with symmetrical 0.14M NaCl solutions. (b) Predicted current-concentration curve at 50mV across the pore. (c) Comparison of equilibrium occupancy at each site *vs.* simulation data with 0.5M NaCl solutions [8]. In doing this fitting we find that  $\Delta\bar{\mu}_{Na,1-4} \sim 2.3, 3.4, 2.8, 2.4kT$ , corresponding to energy barriers of  $\sim 4, 2.9, 3.6, 4kT$  at 0.14M and we find the pore diffusivity to be  $\sim 1.33 \times 10^{-10} \text{m}^2 \text{s}^{-1}$ .

236 0.14M, resulting in a larger ionic current. This is confirmed by predicted current-voltage dependencies  
 237 for 0.25 and 0.5M solutions respectively as showing increases in current; and the current-concentration  
 238 behaviour in (b). In this latter case the bulk solutions are assumed to be symmetrical, with the driving  
 239 force originating from a 50mV voltage drop. This curve clearly demonstrates increasing conduction  
 240 with concentration and we note that the current is relatively small  $< 10\text{pA}$  and is continuing to increase  
 241 even at 2M because the overall energy barrier to enter the pore is large. We expect that these predictions  
 242 can be further refined if more experimental measurements can be made.

#### 243 4.2. Comparison to whole cell data

244 The theory can now be compared to the experimental whole-cell current-voltage recordings  
 245 outlined earlier. In this experiment the data are normalised against the maximal current which is  
 246 calculated when  $-10\text{mV}$  is applied across the pore, and the bath solution contains 0.14M of  $\text{Na}^+$  ions.  
 247 We note that in Fig. 8 (a) this normalisation is with respect to the absolute value of this maximal value.

248 Under experimental conditions only the bath solution was varied. As a result the theoretical  
 249 equilibrium concentration and (chemical potential) used to calculate the conductivity  $\sigma$  and hence  
 250 current varies slightly at each experimental point. This is because they are defined from the average  
 251 concentration (or chemical potential) from both bulk solutions. Since the chemical gradient is calculated  
 252 from the difference in bulk concentrations, we consider the lower limit of bulk concentration to be  
 253 0.1mM rather than 0, to avoid the gradient diverging at low concentrations. Even at with the lowest  
 254 concentration being 0.1mM, the gradient is  $\sim 5kT$  and so at the edge of applicability of our theory.

255 In Fig. 8(a), we plot the normalised current-voltage curves for the range of bath solutions. Overall  
 256 we see good agreement between theory and data, but with two exceptions. NaChBac is a voltage-gated  
 257 channel so that, at negative voltages, the number of open channels is reduced because the open  
 258 probability decreases resulting in a smaller overall current [5,35]. Thus, at voltages below  $-10\text{mV}$   
 259 our current diverges from the experimental data, and hence serves as a prediction of the normalised  
 260 current in a single open channel. This prediction is given by the dashed lines, which we note increase  
 261 in magnitude as voltage becomes more negative because the gradient increases. Furthermore, when  
 262 the bath solution contains no  $\text{Na}^+$  (black dashed curve) we observe poor agreement between theory

and experiment and so highlight the curve with a dashed line. Finally, the inset curve shows the current closest to equilibrium.

The system is in equilibrium when the net current is zero, and this occurs when the applied voltage is equal to the reversal potential  $\phi^{Re}$ . This was measured experimentally and is compared to the theoretical current in (b). In the theory the reversal potential is calculated from,

$$e\phi^{Re} = kT \log(x^L/x^R) \quad (9)$$

where  $L, R$  again refer to the left and right pipette/bath solutions respectively. We see good agreement except when the bath solution contains no  $\text{Na}^+$ . Even, our reduced concentration of 0.1mM yields a reversal potential smaller than -35mV. This is echoed by the current at this concentration which is not in good agreement with the experiment (see the black dashed curve in Fig. 8 (a)). A possible explanation for these disagreements is that, in the absence of  $\text{Na}^+$  in the bath solution,  $\text{K}^+$  ions enter the pore but do not conduct, consequently blocking the pore. Furthermore, at this concentration we are at the limits of applicability because the chemical gradient is still relatively large  $\sim 5kT$ . We plan to discuss this in a future manuscript after further investigations.

In Fig. 9(a) we estimate the effective open probability  $P_{\text{eff}}$ . This is defined relative to the open probability at peak current  $P_{\text{max}}$ , from the ratio of theoretical and experimental current for each of the given concentrations. We neglect the estimate in the absence of  $\text{Na}^+$  because the theoretical current did not agree with experimental data. We observe that  $P_{\text{eff}}$  takes values between 0 and 1.5 except for three concentrations all at +50mV of applied voltage. At 0.126M, 0.138M and 0.14M bath concentration the theoretical current was below the experimental values and in the latter two concentrations of different sign. This produced estimated effective open probabilities,  $P_{\text{eff}}$ , taking the values of 2.5, -15 and -0.5 for the three concentrations respectively (only  $P_{\text{eff}} \sim -0.5$  is shown). Apart from these points however we observe it to be broadly sigmoidal and being 0 at negative voltages as anticipated. We expect, that the actual open probability,  $P_{\text{Open}}$ , can be calculated through the following definition,

$$P_{\text{Open}}(V) = P_{\text{eff}} \times P_{\text{max}}, \quad (10)$$

if the open probability of the maximal current is known.

In Fig. 9 (b) we highlight the current-concentration ( $I - C$ ) behaviour by plotting the  $I - C$  curve at the peak voltage (-10mV). Note that, unlike 8(a), the current is normalised to the maximum current at 0.14M (and not to the absolute value). As expected the theoretical current agrees fairly well with the experimental one except at low concentrations ( $\lesssim 5mM$ ). The curve takes a quasi-linear shape because the current comprises two terms: (1) the conductivity prefactor and (2) the electrochemical gradient. The second term is of the standard form, but our conductivity is a function of the equilibrium bulk chemical potential, which through our derivation must take the averaged concentration between the two bulks and thus slightly varies with bath concentration as well.

## 5. Conclusion and summary

In summary, we have taken the statistical and linear response theory, originally derived in [27] and applied to KcsA and a mutant, and applied it to investigate  $\text{Na}^+$  conduction in NaChBac. Importantly, in order to compare with experimental and simulation data see Fig. 2-3), we needed to extend the theory to take account of a chemical gradient. . In doing so, we derived the conductivity at each site and the total through the pore in the presence of an electrochemical gradient. The main result of the paper is the quantitative predictions of pore function that we make as a function of the energy profile, experimental bulk conditions, and the pore structure. .

In Fig. 7 we compared the theoretical current-voltage and equilibrium site occupancies to experimental and simulation data. This comparison allowed us to extract the following values of  $\Delta\tilde{\mu}_{\text{Na},1-4} \sim 2.3, 3.4, 2.8, 2.4kT$ . At the experimental concentration 0.14M, the 3rd ion faces an energy barrier to enter each site within the pore of  $\sim 4, 2.9, 3.6, 4kT$ . Although these values are

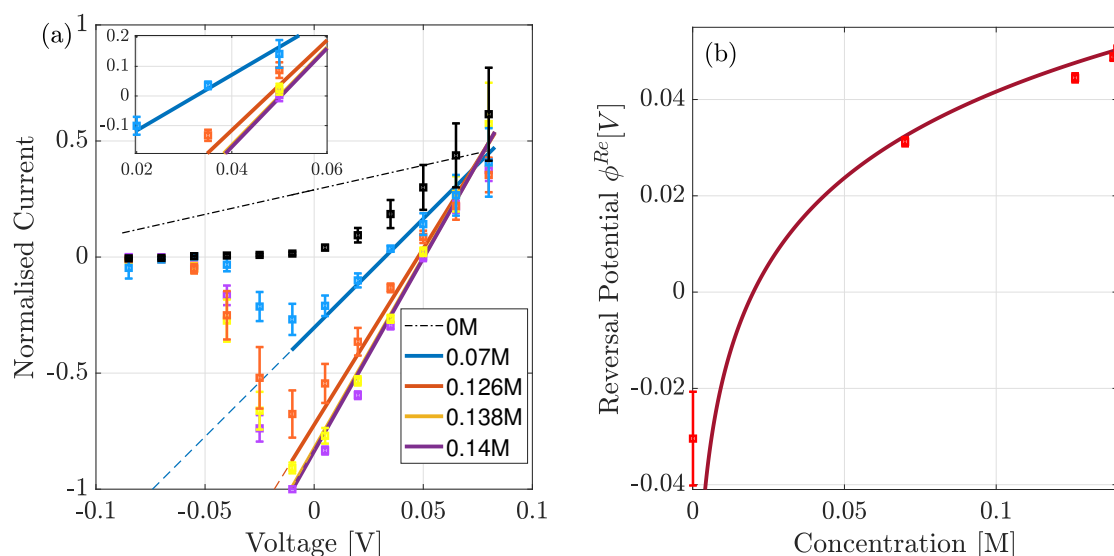


**Figure 8.** (a) Comparison of theoretical (solid line) to experimental (squares) data of normalised (to absolute value) whole-cell current in the presence of an electrochemical gradient, for a range of extra-cellular bulk solutions. The peak occurs at  $-10\text{mV}$ , and below this voltage the current reduces due to the reduction in the open probability. Dashed lines predict the normalised currents if the open probability remained unchanged from the value at the peak current. (b) Theoretical (solid) and experimental (squares) of the reversal potential ( $\phi^{Re}$ ) for a range of concentrations. Theory only differs when the right bulk is absent of  $\text{Na}^+$ .

294 not barrier-less as observed in KcsA [27], they are not expected to be because the experimental  
 295 current is smaller in NaChBac. Furthermore, these parameters lead to barrier heights consistent with  
 296 [8,19]. Using these parameters we have predicted the current for higher concentrations, including the  
 297 current-concentration behaviour with  $50\text{mV}$  of applied voltage and current-voltage dependencies for  
 298  $0.25$  and  $0.5\text{M}$  solutions. As expected both show an increase of current as the bulk solution increases.  
 299 We expect that with more experimental data, we could refined these parameters.

300 In Figs. 8 and 9 we compared the theory to normalised whole-cell data, under the assumption  
 301 that the normalisation effectively renders it a single-channel for the point of comparison. The theory  
 302 was found to be in good agreement with experiment except for when the bath solution was devoid  
 303 of  $\text{Na}^+$ . A possible explanation is that in the absence of  $\text{Na}^+$ ,  $\text{K}^+$  ions enter the pore but do not  
 304 conduct, subsequently blocking the pore. Furthermore, at this concentration we are at the limits of  
 305 applicability because the chemical gradient is still relatively large  $\sim 5kT$ . We plan to investigate this  
 306 in a future manuscript by introducing a far-from equilibrium kinetic model that accounts for both  
 307  $\text{Na}^+$  and  $\text{K}^+$  ions. Such a model was briefly introduced in [19]. However, it failed to account properly  
 308 for the correlations between ions at different sites, and only considered a 2 site pore; and so further  
 309 development is needed.

310 Finally, we expect our theory to be applicable to the study of mixed-valence i.e.  $\text{Na}^+/\text{Ca}^{++}$   
 311 selectivity in NaChBac and related voltage gated  $\text{Ca}^{++}$  channels, alongside artificial nano-pores.

312 We acknowledge valuable discussions with Bob Eisenberg, Igor Khovanov and Aneta Stefanovska.  
 313 The work was funded in part by a PhD Scholarship from the Faculty of Science and Technology of  
 314 Lancaster University, the Engineering and Physical Sciences Research Council (grants EP/M016889/1  
 315 and EP/M015831/1), and by a Leverhulme Trust Research Project Grant RPG-2017-134. Carlo  
 316 Guardiani is currently supported by a project that has received funding from the European Research  
 317 Council (ERC) under the European Union's Horizon 2020 research and innovation programme (grant  
 318 agreement No. 803213)

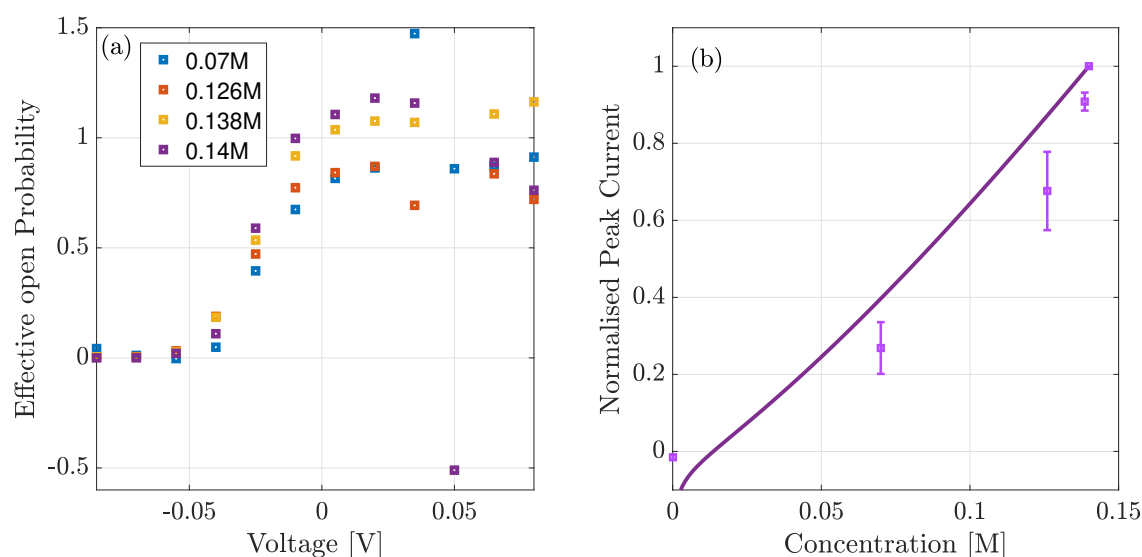


**Figure 9.** (a) Estimated open probability from the ratio of experimental to theoretical current. Below  $-40\text{mV}$  the open probability is close to zero indicating that the channels are closed. (b) Comparison of normalised theoretical current (solid line) and experimental (squares) data *vs.* bulk concentration, at  $-10\text{mV}$  of applied voltage.

319

- 320 1. Zheng, J.; Trudeau, M., Eds. *Handbook of Ion Channels*; CRC Press Taylor & Francis Group: Boca Raton, FL, 2015.
- 321
- 322 2. Hille, B. *Ion Channels Of Excitable Membranes*, 3rd ed.; Sinauer Associates: Sunderland, MA, 2001.
- 323 3. Ashcroft, F. *Ion channels and disease*; Academic press, 1999.
- 324 4. Gao, S.; Valinsky, W.C.; On, N.C.; Houlihan, P.R.; Qu, Q.; Liu, L.; Pan, X.; Clapham, D.E.; Yan, N. Employing NaChBac for cryo-EM analysis of toxin action on voltage-gated  $\text{Na}^+$  channels in nanodisc. *PNAS* **2020**.
- 325
- 326 5. Fedorenko, O.A.; Kaufman, I.K.; Gibby, W.A.; Barabash, M.L.; Luchinsky, D.G.; Roberts, S.K.; McClintock, P.V. Ionic Coulomb blockade and the determinants of selectivity in the NaChBac bacterial sodium channel. *Biochimica et Biophysica Acta (BBA)-Biomembranes* **2020**, p. 183301.
- 327
- 328
- 329 6. Yue, L.X.; Navarro, B.; Ren, D.J.; Ramos, A.; Clapham, D.E. The cation selectivity filter of the bacterial sodium channel, NaChBac. *J. Gen. Physiol.* **2002**, *120*, 845–853.
- 330
- 331 7. Coates, L. Ion permeation in potassium ion channels. *Acta Crystallogr. D* **2020**, *76*, 326–331.
- 332 8. Guardiani, C.; Rodger, P.; Fedorenko, O.; Roberts, S.; Khovanov, I. Sodium Binding Sites and Permeation Mechanism in the NaChBac Channel: A Molecular Dynamics Study. *J. Chem. Theor. Comp.* **2016**, p. 10.1021/acs.jctc.6b01035. doi:10.1021/acs.jctc.6b01035.
- 333
- 334
- 335 9. Guardiani, C.; Fedorenko, O.A.; Roberts, S.K.; Khovanov, I.A. On the selectivity of the NaChBac channel: an integrated computational and experimental analysis of sodium and calcium permeation. *Physical Chemistry Chemical Physics* **2017**, *19*, 29840–29854.
- 336
- 337
- 338 10. Guardiani, C.; Fedorenko, O.A.; Khovanov, I.A.; Roberts, S.K. Different roles for aspartates and glutamates for cation permeation in bacterial sodium channels. *Biochimica et Biophysica Acta (BBA)-Biomembranes* **2019**, *1861*, 495–503.
- 339
- 340
- 341 11. Chakrabarti, N.; Ing, C.; Payandeh, J.; Zheng, N.; Catterall, W.A.; Pomès, R. Catalysis of  $\text{Na}^+$  permeation in the bacterial sodium channel NaVAb. *Proceedings of the National Academy of Sciences* **2013**, *110*, 11331–11336, [\[https://www.pnas.org/content/110/28/11331.full.pdf\]](https://www.pnas.org/content/110/28/11331.full.pdf). doi:10.1073/pnas.1309452110.
- 342
- 343
- 344 12. Ulmschneider, M.B.; Bagnéris, C.; McCusker, E.C.; DeCaen, P.G.; Delling, M.; Clapham, D.E.; Ulmschneider, J.P.; Wallace, B.A. Molecular dynamics of ion transport through the open conformation of a bacterial voltage-gated sodium channel. *Proceedings of the National Academy of Sciences* **2013**, *110*, 6364–6369, [\[https://www.pnas.org/content/110/16/6364.full.pdf\]](https://www.pnas.org/content/110/16/6364.full.pdf). doi:10.1073/pnas.1214667110.
- 345
- 346
- 347

- 348 13. Root, M.J.; MacKinnon, R. Two identical noninteracting sites in an ion channel revealed by proton transfer.  
349 *Science* **1994**, *265*, 1852–1856.
- 350 14. Corry, B.; Allen, T.W.; Kuyucak, S.; Chung, S.H. Mechanisms of permeation and selectivity in calcium  
351 channels. *Biophysical Journal* **2001**, *80*, 195–214.
- 352 15. Furini, S.; Barbini, P.; Domene, C. Effects of the protonation state of the EEEE motif of a bacterial  
353 Na<sup>+</sup>-channel on conduction and pore structure. *Biophysical Journal* **2014**, *106*, 2175–2183.
- 354 16. Corry, B.; Thomas, M. Mechanism of ion permeation and selectivity in a voltage gated sodium channel. *J.*  
355 *Am. Chem. Soc.* **2012**, *134*, 1840–1846.
- 356 17. Boiteux, C.; Vorobyov, I.; Allen, T.W. Ion conduction and conformational flexibility of a bacterial  
357 voltage-gated sodium channel. *Proceedings of the National Academy of Sciences* **2014**, *111*, 3454–3459.
- 358 18. Damjanovic, A.; Chen, A.Y.; Rosenberg, R.L.; Roe, D.R.; Wu, X.; Brooks, B.R. Protonation state of the  
359 selectivity filter of bacterial voltage-gated sodium channels is modulated by ions. *Proteins: Structure,*  
360 *Function, and Bioinformatics* **2020**, *88*, 527–539.
- 361 19. Gibby, W.A.T.; Barabash, M.; Guardiani, C.; Luchinsky, D.; Fedorenko, O.; Roberts, S.K.; McClintock, P.V.E.  
362 Theory and experiments on multi-ion permeation and selectivity in the NaChBac ion channel. *Fluctuation*  
363 *and Noise Letters* **2019**, *18*, 1940007.
- 364 20. Kaufman, I.; McClintock, P.; Eisenberg, R. Coulomb blockade model of permeation and selectivity in  
365 biological ion channels. *New J. Phys.* **2015**, *17*, 083021.
- 366 21. Krems, M.; Di Ventra, M. Ionic Coulomb blockade in nanopores. *J. Phys. Condens. Matter* **2013**, *25*, 065101.
- 367 22. Yesylevskyy, S.O.; Kharkyanen, V.N. Barrier-less knock-on conduction in ion channels: peculiarity or  
368 general mechanism? *Chem. Phys.* **2005**, *312*, 127–133.
- 369 23. Feng, J.; Liu, K.; Graf, M.; Dumcenco, D.; Kis, A.; Di Ventra, M.; Radenovic, A. Observation of ionic  
370 Coulomb blockade in nanopores. *Nature Mater.* **2016**, *15*, 850 – 855.
- 371 24. Chernev, A.; Marion, S.; Radenovic, A. Prospects of Observing Ionic Coulomb Blockade in Artificial Ion  
372 Confinements. *Entropy* **2020**, *22*, 1430.
- 373 25. Zhou, M.; MacKinnon, R. A mutant KcsA K<sup>+</sup> channel with altered conduction properties and selectivity  
374 filter ion distribution. *J. mol. biol.* **2004**, *338*, 839–846.
- 375 26. Tilegenova, C.; Cortes, D.M.; Jahovic, N.; Hardy, E.; Hariharan, P.; Guan, L.; Cuello, L.G. Structure, function,  
376 and ion-binding properties of a K<sup>+</sup> channel stabilized in the 2,4-ion bound configuration. *Proc. Nat. Acad.*  
377 *Sci. (USA)* **2019**, *116*, 16829–16834.
- 378 27. Gibby, W.; Barabash, M.; Guardiani, C.; Luchinsky, D.; McClintock, P. Physics of selective conduction and  
379 point mutation in biological ion channels. *arXiv preprint arXiv:2010.08450* **2020**.
- 380 28. Pettersen, E.F.; Goddard, T.D.; Huang, C.C.; Couch, G.S.; Greenblatt, D.M.; Meng, E.C.; Ferrin, T.E.  
381 UCSF Chimera—a visualization system for exploratory research and analysis. *J. Comput. Chem.* **2004**,  
382 *25*, 1605–1612.
- 383 29. Kubo, R. Statistical-mechanical theory of irreversible processes. I. General theory and simple applications  
384 to magnetic and conduction problems. *Journal of the Physical Society of Japan* **1957**, *12*, 570–586.
- 385 30. Kubo, R. The fluctuation-dissipation theorem. *Reps, Progr. Phys.* **1966**, *29*, 255.
- 386 31. Zwanzig, R. *Nonequilibrium statistical mechanics*; Oxford University Press, 2001.
- 387 32. Krems, M.; Di Ventra, M. Ionic Coulomb blockade in nanopores. *J. Phys. Condens. Matter* **2013**, *25*, 065101.
- 388 33. Tieleman, D.P.; Biggin, P.C.; Smith, G.R.; Sansom, M.S.P. Simulation approaches to ion channel  
389 structure-function relationships. *Quart. Rev. Biophys.* **2001**, *34*, 473–561.
- 390 34. Roux, B.; Allen, T.; Berneche, S.; Im, W. Theoretical and computational models of biological ion channels.  
391 *Quart. Rev. Biophys.* **2004**, *37*, 15–103.
- 392 35. Jo, A.; Hoi, H.; Zhou, H.; Gupta, M.; Montemagno, C.D. Single-molecule study of full-length NaChBac by  
393 planar lipid bilayer recording. *PloS one* **2017**, *12*, e0188861.